Smart Structures and Systems, *Vol. 29, No. 4 (2022) 577-588*
https://doi.org/10.12989/sss.2022.29.4.577

Monitoring and vibration control of a fluid catalytic cracking unit

Ronaldo C. Battista [1a], Wendell D. Varela*[2] and Igor Braz N. Gonzaga [2b]

[1] *COPPE Engineering Institute, Universidade Federal do Rio de Janeiro, Controllato Ltd., Brazil*
[2] *COPPE Engineering Institute, Universidade Federal do Rio de Janeiro, C. Postal 68506, CEP 21941-972, Rio de Janeiro/RJ, Brazil*

(*Received August 18, 2021, Revised November 11, 2022, Accepted November 23, 2021*)

Abstract. Oil refineries' Fluid Catalytic Cracking Units (FCCU) when in full operation may exhibit strong fluid dynamics caused by turbulent flow in the piping system that may induce vibrations in other mechanical and structural components of the Unity. This paper reports on the experimental-theoretical-computational program performed to get the vibration properties and the dynamic response amplitudes to find out alternative solutions to attenuate the excessive vibrations that were causing fatigue fractures in components of the bottle like reactor-regenerator of an FCC unit in operation in an existing oil refinery in Brazil. Solutions to the vibration problem were sought with the aid of a 3D finite element model calibrated with the results obtained from experimental measurements. A short description of the found solutions is given and their effectiveness are shown by means of numerical results. The solutions were guided by the concepts of structural stiffening and dynamic control performed by a nonlinear pendulum controller whose mechanical design was based on parameters determined by means of a parametric study carried out with 2D and 3D mathematical models of the coupled pendulum-structure system. The effectiveness of the proposed solutions is evaluated in terms of the fatigue life of critical welded connections.

Keywords: computational modelling; dynamics; passive device; structural monitoring; vibration control

1. Introduction

Fluid catalytic cracking unit (FCCU) is the most common conversion technology in the oil refinery industry. This chemical process uses heat and catalytic to refine the petroleum into smaller-chain hydrocarbons that are common commercial products like gasoline, kerosene and diesel fuels. (Letzsch 2015, Medeiros *et al*. 2010, Vogt and Weckhuysen 2015). The FCC unit is composed by several equipment such as: reactor, regenerator, expansion vessel, orifices chamber, risers and storage silos.

The industrial process of refining the petroleum consists in three main steps: reaction, product separation and regeneration (Pinheiro *et al*. 2011, Ali *et al*. 2005). In the first step, the feedstock is lifted up through the riser pipe to the reactor. In the riser, the feedstock is combined with hot catalyst material (≈550°C) and it is vaporized (Vogt and Weckhuysen 2015). The catalyst used is a small grain size solid powder fluidized by steam in high temperatures (Medeiros *et al*. 2010). In the second step, the mixture enters in a solid-gas separator, the cracked gases are fractionated, the catalyst and residues are deposited at the bottom of the equipment by gravity, and it is transported to the regenerator. The third step consists in burn off the coke in the regenerator. The coke is a certain amount of carbon formed in the first step and deposited in the catalyst surface causing its deactivation (Speight 2006). As a product of the third step, the carbon dioxide is released, the catalyst is regenerated and continuously reused. (Pinheiro *et al*. 2011, Vogt and Weckhuysen 2015).

The large dimension of the equipments composing the bottle like FCC unit (over 60 m of height and 10-12 m in diameter) configures a scenario prone to high amplitudes of vibrations. These vibrations are produced by environmental loads and forces generated in the internal operating process, which in the focused FCC unit was mainly caused by turbulent fluid-flow in the piping system.

Undesirable amplitudes of vibrations in structural systems shall be avoided. Structural stiffening has been widely used by engineers as design solution to reduce vibrations in existing structures (Duran *et al*. 2018, Zhu *et al*. 2021); although, in certain cases, this may lead to inappropriate dimensions of structural components, undesirable increase of mass or to cost-benefit trap. Alternatively, passive dynamic devices are an efficient and inexpensive solution besides requiring low maintenance (An *et al*. 2015, Alih *et al*. 2018, Lin *et al*. 2019, Sharma *et al*. 2019, Shahabi *et al*. 2020, Zhang *et al*. 2021, Cao *et al*. 2021).

Other researchers (Nguyen *et al*. 2014) have investigated the performance of two alternative measures to reduce the vibrations in a built structure: (i) structural stiffening and (ii) passive control devices coupled with the structure. The authors concluded that the latter solution has clear advantages over the former; its performance is by far superior and in general feasible, lower cost and non-intrusive. Pinheiro and Battista (2012) evaluated the efficiency of a nonlinear spatial pendulum and concluded that a small value (at most 5%) of the ratio between the

*Corresponding author, Ph.D., Professor,
E-mail: wendell@fau.ufrj.br
[a] Professor, E-mail: battista@coc.ufrj.br
[b] Ph.D. Student, E-mail: igor.gonzaga@coc.ufrj.br

ISSN: 1738-1584 (Print), 1738-1991 (Online)

mass of the controller and the main vibration modal mass of the structure may lead to great reductions (up to 95%) of the vibration amplitudes. Zahrai and Froozanfar (2019) noted that the effectiveness of a TMD stablishes in its maximum value to a ratio of mass of just 1%. Sun *et al*. (2018) reported a mitigation of fatigue damage on an offshore wind tower by up 90% using a 3D pendulum tuned mass damper with a mass ratio of just 2%.

According to Battista *et al*. (2018), a nonlinear spatial pendulum controller (NLP) is particularly appropriate to attenuate oscillations of low frequency fundamental bending mode of tall and slender tower structures, as for example telecommunication towers. Ikeda *et al*. (2017) pointed out that a spherical NLP is most indicated to control planar vibration amplitudes in any horizontal direction.

This paper reports on the extensive program of experimental measurements that was carried out to collect data for dynamic identification of the FCC unit (vibration frequencies and mode shapes) and to pick up the high amplitudes of vibration that led to frequent interruption of the industrial production.

A 3D finite element model was constructed and calibrated with the experimentally obtained vibration frequencies and mode shapes.

The achieved numerical and experimental results led to the conclusion that the procedures adopted for the FCC unit operation was the main source of the vibration problem in the reactor-regenerator tower of the FCC unit.

A two-fold solution was proposed to attenuate vibration amplitudes and to reduce the susceptibility to fatigue failure: (i) the installation of a non-linear pendulum (NLP) controller at the top of the bottle-like reactor-regenerator tower; (ii) the stiffening of the "neck" that connects the reactor to the regenerator (Fig. 1). The contributions of each of the two solutions to enhance fatigue life of a critical connection welded in the tower neck are evaluated.

The optimum parameters of the NLP were found by means of a parametric study using 2D and 3D mathematical models which are described herein. Other numerical approaches for studying pendulum controllers were also successfully applied by Gerges and Vickery (2005), Roffel *et al*. (2013), Fallahpasand *et al*. (2015), Sado *et al*. (2016), Wang *et al*. (2020).

2. Brief description of the FCC unit structural system

The FCC unit structural system is composed by an assemblage of the industrial equipment components, their reinforced concrete support structure and foundation caissons. The bottle like-tower structure has a height of 60 m and its bottom and upper diameter are 10 m and 12 m, respectively.

All equipment parts are composed by steel pipes and cylindrical shells with an inner refractory mortar layer for thermal isolation clamped to the steel walls by welded connectors. The temperature inside the pipes reaches 600°C and outside, due to the mortar layer, 200°C. Fig. 1 shows one view and illustrates the components of the FCC unit, Table 1 presents the properties of the materials, while Table 2 presents the geometrical and physical parameters.

The reinforced concrete frame structure supporting the FCC unit is composed by very stocky beams and columns, loading the foundation of reinforced concrete cylindrical caissons, 1.8 to 3.1 m in diameter and length varying from 10.6 m to 14.5 m needed to cross the various layers of soft clay till reaching a resistant soil.

(a) View of the compound parts

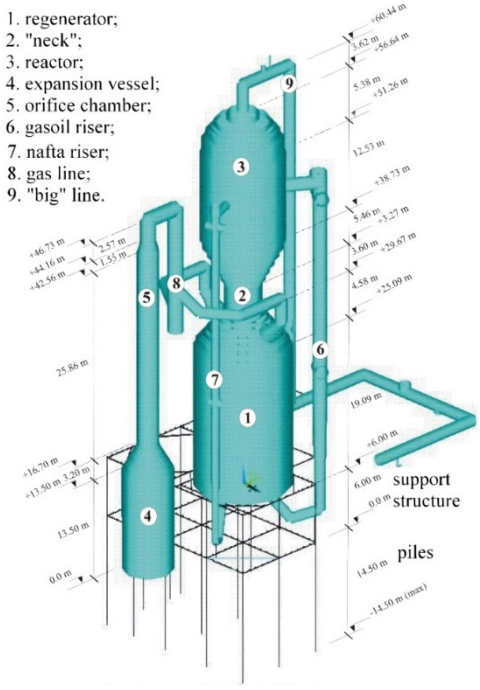

(b) Description of the FCC unit elements

Fig. 1 Fluid catalytic cracking unit (FCC unit) of Cubatão Refinery, São Paulo State, Brazil

Table 1 Experimental and numerical modes of the FCCU

Material	Elasticity modulus (MPa)	Poisson's ratio	Density (kg/m³)	Operating process (°C)
Steel	204000	0.29	7850	≤ 200
Mortar	8560-30300	0.20	1300-2700	200 ≤ T ≤ 600
Concrete	29500	0.20	2500	20 ≤ T ≤ 40

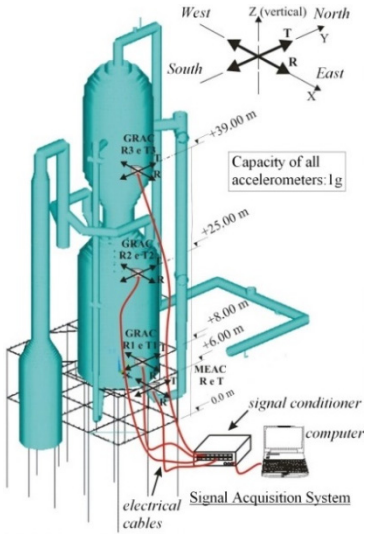

Fig. 2 Arrangement of the accelerometers at the reactor-regenerator tower

3. Experimental measurements

3.1 Brief description of the instrumentation

The FCC unit is located in a region of coastal lowland and its foundation is based on clay soil which is characterized by high compressibility and low strength. The physical properties of the soil may vary depending on its humidity. These changes can cause differences in the flexibility and damping of the coupled soil-structure system, and, therefore, in the values of the natural frequencies and in the amplitudes of dynamic responses, as it is desribed in Section 3.2. As the rain volume activity varies with the season (in the summer season the rain volume is the highest and in winter the lowest), measurement campaigns were carried out during several weeks in two distinct seasons over one year.

Table 2 Geometrical and physical parameters of the FCC elements

Element	Outside diameter (cm)		Thickness (cm)		Mass (t)
	Steel	Mortar	Steel	Mortar	
Reactor (01)	1214.0	1209.8	2.1-2.5	10.2	1250
"Neck" (02)	473.5	465.5	4.3	10.2	
Regenerator (03)	1047.6	1037.0	4.3-5.3	10.2	
Expansion Vessel (04)	643.6	640.0	1.8	10.2	166
Orifice chamber (05)	272.2	270.0	1.1	7.6-12.7	
Gasoil riser (06)	182.8	179.8	1.3-2.5	7.6-12.7	198
Nafta riser (07)	106.6	101.6	1.3-2.5	7.6-12.7	107
Gas line (08)	234.4	230.0	1.0-2.2	7.6-12.7	67
"Big" line (09)	152.4	167.6	1.3-2.5	7.6	61
Storage Silo O-2401	-	-	-	-	296
Storage Silo O-2402	-	-	-	-	1345

Thirty-one waterproof accelerometers (model ASW) from Kyowa Co (capacity of 1 g, 2 g, 5 g and 20 g) were installed on the FCC unit at different positions and arrangements in each campaign. Fig. 2 shows an example of arrangement of accelerometers installed on the bottle like reactor-regenerator unit.

The accelerometers were mounted in aluminum cantilever pieces that were fixed to the structure steel wall. Pieces of glass wool thermal blanket were wrapped on each accelerometer as shown in Fig. 3(a) to attenuate the effects of high temperatures (up to 200°C), that would damage it.

The signal acquisition system indicated in Fig. 2 is composed by two signal conditioners model ADS2000 (made in Brazil by Lynx Ltd.) with an analogical to digital board and 16 channels each. Different combinations of points per second (pps) digital signal acquisition and of operational conversion rate (68%-75% related to the volume of catalytic) were employed in each campaign.

3.2 Main results

It was noticed that changes in volumes rates of catalyst did not affect the low frequency global motion amplitudes

(a) Accelerometers GRACT and R2 (Fig. 2)

(b) Zoom of 3 accelerometers assemblage

Fig. 3 Accelerometers protected against high temperature with fiber glass wool

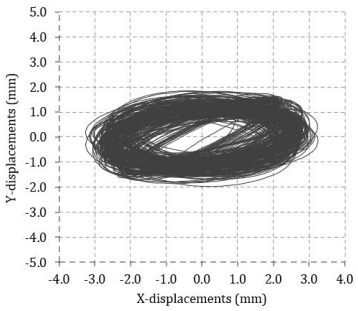

(a) Planar motion at level 39 m

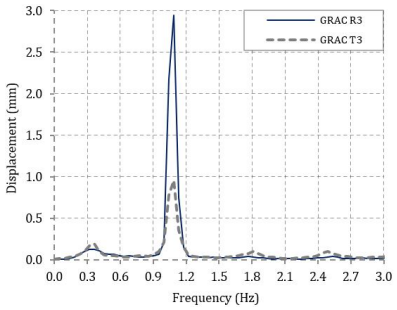

(b) FFT of the measured signals

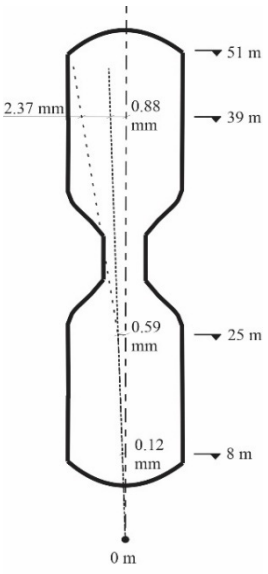

(c) Along the height

Fig. 4 Displacement amplitudes of the bottle like reactor-regenerator unit

of the bottle like reactor-regenerator unit, but the high frequency vibrations at the orifices chamber (Fig. 1(b)).

All the dominant mode shapes were identified. The two first dominant mode shapes are characterized by lateral bending modes in the directions YZ and XZ of the bottle-like unit (1.06 Hz and 1.07 Hz, respectively) that induces the motion of the other structural components of the superstructure (risers, expansion vessels, orifices chamber, "big" line, etc.).

The bottle like reactor-regenerator unit oscillated in an orbital trajectory, as shown in Fig. 4(a), with displacements in east-west direction reaching ±3.25 mm at level 39 m. The maximum and the minimum measured displacements in two distinct seasons over the year were respectively ±4.5 mm and ±0.5 mm, the first measured value for a saturated soil condition and the second for a dry soil condition.

Fig. 4(b) shows the frequency spectra of the displacement time responses at the top of the bottle-like tower in bending motion in both XZ and YZ planes, which dominates the dynamic response of the structure together with all components of the FCC unit.

The overall mode shape of the bottle like reactor-regenerator unit (saturated soil condition) as shown in Fig. 4(c) is composed by two contributing mode shapes: one is its motion like an inverted pendulum allowed by the base/foundation flexibility, and the other the local bending of the "neck", being this the larger contribution to the overall mode shape. This led to the conclusion that the

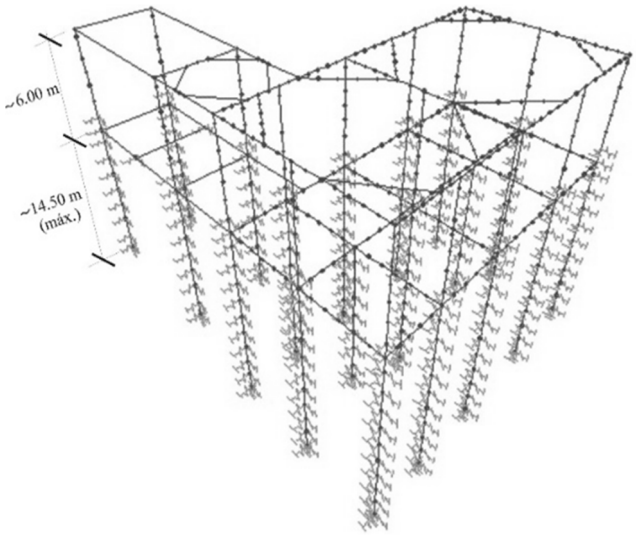

Fig. 5 Model of the RC support frame structure and foundations

Table 3 Experimental and numerical modes of the FCCU

Mode	Frequency (Hz)		Description of the modes and the components of the FCCU involved on it
	Experimental	Numerical	
1	1.06 ± 0.04	0.94	1° bending mode of the bottle-like tower in the YZ plan involving all components of the FCC unit and weight counter-balance arm of the risers.
2	1.07 ± 0.04	1.01	1° bending mode of the bottle-like tower in the XZ plan involving all components of the FCC unit, supports and weight counter-balance arm of the risers.
3	1.08 ± 0.04	1.10	1° bending mode of the bottle-like tower in the XZ plan involving all components of the FCC unit and weight counter-balance arm of the risers.
5	1.08 ± 0.04	1.28	Lateral bending mode coupled with vertical bending mode and weight counter-balance arm of the gasoil riser, induced by the fundamental motion of the bottle-like tower.
9	1.77 ± 0.04	1.58/1.71	1° bending mode of the bottle-like tower in the YZ plan involving all components of the FCC unit and supports.
15	2.14 ± 0.04	1.92	1° transverse bending of the orifice chamber in the XZ plan
19	2.75 ± 0.04	2.50/2.59	1° radial bending mode of the orifice chamber tower in the YZ plan, bending of the gasoil riser and vertical bending of the weight counter-balance arm of gasoil riser.

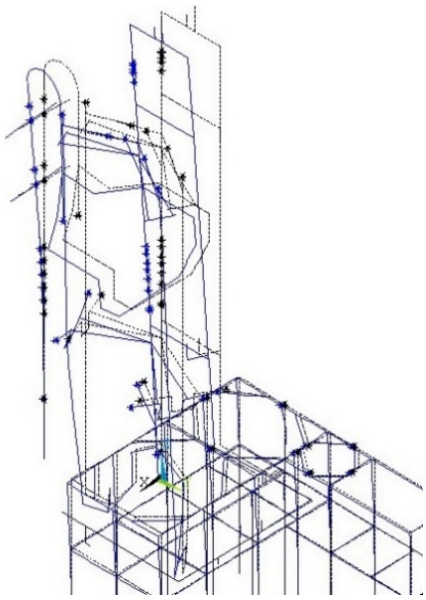

Fig. 6 Dominant mode shape of complete model

"neck" needed special attention, particularly related to fatigue of the welded connections of the curved steel plates.

4. Numerical Modeling

A numerical 3D finite element model of the FCC unit, its components, the reinforced concrete support structure and the caissons foundation were all modelled with 3D spatial frame elements. The soil-structure interaction was considered by modelling the soil as springs along the length of the caissons, as shown in Fig. 5. The stiffnesses of the springs were estimated from the soil survey profiles obtained by means of percussion and drilling tests.

The contribution of the mortar layer to the wall stiffness of the FCC unit steel components was considered in the model. The composite shell wall structure stiffness increased around 57% and 40%, respectively for the orifice chamber and the bottle-like unit. Thermo-mechanics expansion joints were also simulated in the model to evaluate changes in natural frequencies and mode shapes under thermic stress generated by the operational process of the FCC unit. It was found that these expansion joints have negligible effects on the modal properties of the structure.

Table 3 shows a summarized description of the vibration modes of the FCC unit, the involved components and equipment and a comparison between the experimental and the theoretical vibration frequencies. The first dominant mode shape is described as the bending of the reactor-regenerator unit in the YZ plane involving all equipment, the supporting structure and foundations. The second bending vibration mode shape in the XZ plane has similar description (see Fig. 6). These two dominant vibration modes played an essential role in the design of the control system, as it had to attenuate vibrations of the reactor-regenerator unit in both directions simultaneously.

5. Improvement of the dynamic behavior

To enhance fatigue life and to reduce the low frequency (1-2 Hz) oscillation amplitudes of the reactor-regenerator tower, due to the piston effect caused by forces induced by the fluid-flow and collision of the carried solid particles with the FCC unit pipes' wall, two different solutions were tested and their performance were further evaluated: structural stiffening and strengthening of the "neck" and/or installation of a passive control system at the top of the bottle-like tower.

The first proposed solution to be applied was the installation of four curved steel tubular struts (800 mm of

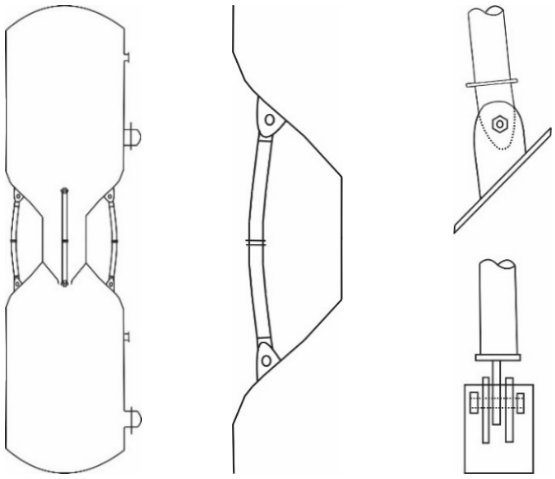

(a) Schematics (b) Detail of one strut (c) Strut support

Fig. 7 Stiffening and strengthening of the "neck" of the reactor-regenerator tower

external diameter and 10 mm of thickness to the "neck" that connects the reactor and regenerator parts), as illustrated in Fig. 7. The struts were properly fabricated with a curved shape to accommodate the high amplitudes of thermal variations in the bottle-like tower.

The second proposed solution was a nonlinear spatial pendulum controller with a torus-like shape installed on the top of the bottle-like tower. The torus is a steel pipe filled with sand and suspended by 8 simple pin-ended rods hanging from tubular curved cantilevered frames fixed in 8 points along the perimeter of a tubular ring welded to the top spherical cap, as illustrated in Figs. 8(a)-(b).

6. Theoretical modelling of the nonlinear pendulum device

The optimum parameters of the controller were determined by using a 2D and a 3D mathematical model to represent the motion of the coupled system pendulum-structure.

6.1 2D mathematical model

The mathematical model of the coupled structure-pendulum in the plan is represented by a spring-mass-damper system as indicated in Fig. 9. The formulation is based on the dynamic equilibrium of the system utilizing the Lagrange's equation as shown in Eq. (1).

$$\frac{d}{dt}\frac{\partial T}{\partial \dot{q}_i} - \frac{\partial T}{\partial q_i} + \frac{\partial V}{\partial q_i} + \frac{\partial E_d}{\partial \dot{q}_i} = Q_i \tag{1}$$

where T is the kinetic energy, V is the potential energy, E_d is the dissipation energy, Q_i is the external force and q_i is the generalized coordinate of the system.

The terms in Eq. (1) can be written as follow in Eqs. (2)-(4)

$$T = \frac{1}{2}m_s\dot{x}^2(t) + \frac{1}{2}m_p v^2(t) \tag{2}$$

in which: $\dot{x}$ is the velocity of the structure, m_s is the modal mass of the structure in the direction evaluated, m_p is the pendulum mass, and v is the tangential speed of the pendulum that can be rewritten in terms of the velocity of the structure and the rotational velocity of the pendulum.

$$V = \frac{1}{2}k_s x^2(t) + m_p g h + \frac{1}{2}k_p\theta^2(t) \tag{3}$$

k_s and k_p are the modal stiffness of the structure in the direction assessed and the modal stiffness of the pendulum, respectively. g is gravity acceleration and h is the height reached by the pendulum mass in relation to the static equilibrium position.

$$E_d = \frac{1}{2}c_s\dot{x}^2(t) + \frac{1}{2}c_p\theta^2(t) \tag{4}$$

where the variables c_s and c_p are respectively the modal damping of the structure and of the controller.

Assuming x as the generalized coordinate representing the displacements of the structure and θ as the generalized coordinate representing the rotation of the pendulum device and deriving Eqs. (2)-(4) according to the terms indicated in

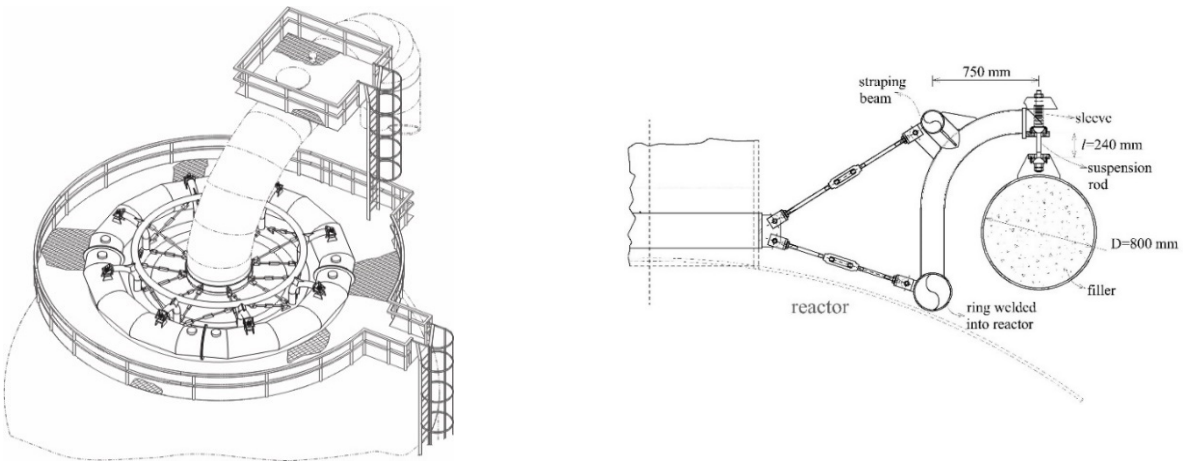

(a) Perspective view (b) Details

Fig. 8 Nonlinear pendulum control system (NLP)

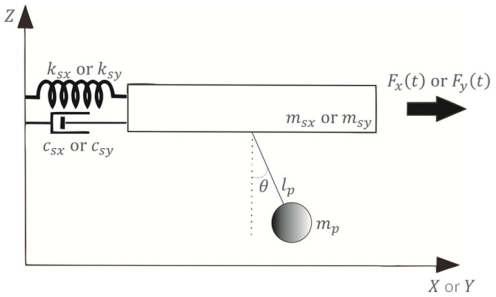

Fig. 9 2D representation of the pendulum-structure system

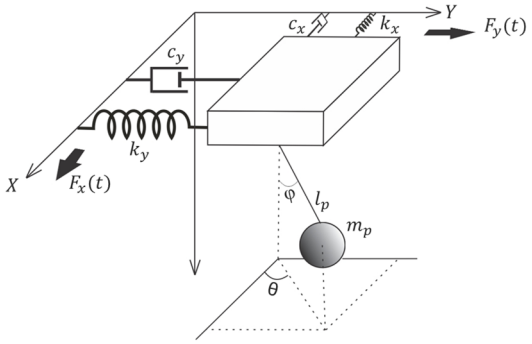

Fig. 10 3D representation of the pendulum-structure system

Eq. (1), in relation to the structure's generalized coordinate (x), it becomes

$$\frac{\partial T}{\partial \dot{x}(t)} = m_s\dot{x}(t) + m_p[\dot{x}(t) + l\dot{\theta}(t)\cos\theta\,(t)] \tag{5}$$

$$\frac{d}{dt}\frac{\partial T}{\partial \dot{x}(t)} = m_s\ddot{x}(t) + m_p[\ddot{x}(t) + l\ddot{\theta}(t)cos\theta(t) - l\dot{\theta}^2(t)sin\theta(t)] \tag{6}$$

$$\frac{\partial V}{\partial x(t)} = k_s x(t) \tag{7}$$

$$\frac{\partial T}{\partial x(t)} = 0 \tag{8}$$

$$\frac{\partial E_d}{\partial x(t)} = c_s x(t) \tag{9}$$

Rearranging Eqs. (5)-(9) according to the Lagrange's formulation indicated in Eq. (1) and considering a generic external force $F(t)$ acting on the system, the structure's motion can be determined by solving Eq. (10)

$$[m_s + m_p]\ddot{x}(t) + c_s\dot{x}(t) + k_s x(t) + m_p l[\ddot{\theta}(t)cos\theta(t) - \dot{\theta}^2(t)sin\theta(t)] = F(t) \tag{10}$$

The equation of the pendulum's motion can be determined by the partial derivatives of the energy equations in relation to θ, resulting in Eq. (11)

$$m_p l^2\ddot{\theta}(t) + c_p\dot{\theta}(t) + k_p\theta(t) + m_p lgsin\theta(t) + m_p l\ddot{x}(t)cos\theta(t) = 0 \tag{11}$$

Rewriting Eqs. (10) and (11) in a matrix form, the coupled equation of the pendulum-structure motion may be expressed by Eq. (12)

$$\begin{bmatrix}(m_s+m_p) & m_p lcos\theta(t)\\ m_p lcos\theta(t) & m_p l^2\end{bmatrix}\begin{Bmatrix}x(t)\\ \theta(t)\end{Bmatrix} + \begin{bmatrix}c_s & m_p l\dot{\theta}sin\theta(t)\\ 0 & c_p\end{bmatrix}\begin{Bmatrix}x(t)\\ \theta(t)\end{Bmatrix} + \begin{bmatrix}c_s & 0\\ 0 & k_p\end{bmatrix}\begin{Bmatrix}x(t)\\ \theta(t)\end{Bmatrix} + \begin{Bmatrix}0\\ m_p glsin\theta(t)\end{Bmatrix} = \begin{Bmatrix}F(t)\\ 0\end{Bmatrix} \tag{12}$$

It is important to notice the non-linearity in Eq. (12) present in both mass and damping matrices of the coupled system equations.

6.2 3D mathematical model

The mathematical model that represents the coupled structure-pendulum system in spatial coordinates is expressed in terms of 4 DoF, as shown in Fig. 10. Two DoF, x and y are related to the motion of the structure in the horizontal plan. The others, φ and θ, are the rotation angle measured from the Z-axis with the rod of the pendulum and the angle formed between the rod projection in xy-plan with X-axis, respectively.

The time dependent variables of the system are defined as x, y and z and expressed by Eq. (13); being z the coordinate relative to the displacements of the pendulum mass in the relation to the vertical axis, while x and y refers to the structure's displacements in the directions X and Y.

$$\begin{cases} x(t) = x_0 + lsin\varphi(t)cos\theta(t) \\ y(t) = y_0 + lsin\varphi(t)sin\theta(t) \\ z(t) = lcos\varphi(t) \end{cases} \tag{13}$$

x_0 and y_0 are the initial displacement of the structure at the point where the pendulum rod is fixed.

The kinetic energy, potential energy and dissipation energy of the system are given by the Eqs. (14)-(16)

$$T = \frac{1}{2}m_{sx}\dot{x}^2(t) + \frac{1}{2}m_{sy}\dot{y}^2(t) + \frac{1}{2}m_p v^2(t) \tag{14}$$

where m_{sx} and m_{sy} are the modal mass of the structure in X and Y directions, respectively.

$$U = \frac{1}{2}k_{sx}x^2(t) + \frac{1}{2}k_{sy}y^2(t) + m_p gh + \frac{1}{2}k_p\varphi^2(t) \tag{15}$$

k_{sx} and k_{sy} are the stiffness in X and Y directions, respectively.

$$E_d = \frac{1}{2}c_{sx}\dot{x}^2(t) + \frac{1}{2}k_{sy}\dot{y}^2(t) + \frac{1}{2}c_p\dot{\varphi}^2(t) \tag{16}$$

c_{sx} and c_{sy} are the modal damping of the structure in X and Y directions, respectively.

Analogously to the mathematical development of the 2D nonlinear pendulum controller, the parcels of energy given

in Eqs. (14)-(16) are rewritten in function of the DoFs of the mechanical system and it is derived in relation to the respective generalized coordinate of the system. Then, they are rearranged in accordance with the Lagrange's equation resulting in a coupled system of differential equations, in which each equation refers to one of the generalized coordinates of the system.

Considering that a generic external force represented by the components F_x and F_y is actuating on the horizontal plan, the mathematical model representing the motion of the 3D pendulum-mass and the motion of the structure in plan can be expressed by the system of Eq. (17)

$$\begin{bmatrix} (m_{sx}+m_p) & 0 & bcos\theta(t) & -acos\theta(t) \\ 0 & (m_{sy}+m_p) & bsin\theta(t) & acos\theta(t) \\ bcos\theta(t) & bsin\theta(t) & m_p l^2 & 0 \\ -asin\theta(t) & acos\theta(t) & 0 & m_p alsin\varphi(t) \end{bmatrix} \begin{Bmatrix} \ddot{x}(t) \\ \ddot{y}(t) \\ \ddot{\varphi}(t) \\ \ddot{\theta}(t) \end{Bmatrix}$$
$$+ \begin{bmatrix} c_{sx} & 0 & -a\dot{\varphi}(t)cos\theta(t) & -a\dot{\theta}(t)cos\theta(t) \\ 0 & c_{sy} & -a\dot{\varphi}(t)sin\theta(t) & -a\dot{\theta}(t)sin\theta(t) \\ 0 & 0 & c_p & -alcos\varphi(t)\dot{\theta}(t) \\ 0 & 0 & 2al\dot{\theta}(t)cos\varphi(t) & alsin\varphi(t) \end{bmatrix} \begin{Bmatrix} \dot{x}(t) \\ \dot{y}(t) \\ \dot{\varphi}(t) \\ \dot{\theta}(t) \end{Bmatrix} \tag{17}$$
$$+ \begin{bmatrix} k_{sx} & 0 & 0 & 0 \\ 0 & k_{sy} & 0 & 0 \\ 0 & 0 & k_p & 0 \\ 0 & 0 & 0 & 0 \end{bmatrix} \begin{Bmatrix} x(t) \\ y(t) \\ \varphi(t) \\ \theta(t) \end{Bmatrix} + \begin{Bmatrix} -2b\dot{\varphi}(t)\dot{\theta}(t)sin\theta(t) \\ 2b\dot{\varphi}(t)\dot{\theta}(t)sin\theta(t) \\ ag \\ 0 \end{Bmatrix} = \begin{Bmatrix} F_x(t) \\ F_y(t) \\ 0 \\ 0 \end{Bmatrix}$$

where $a = m_p lsin\varphi(t)$ and $b = m_p lcos\varphi(t)$.

As in Eq. (12), it is noted in the system of Eq. (17) the nonlinear terms involving the DoFs, or in other words, the strong coupling between the motions of the pendulum mass and the structure.

Another important aspect to be pointed out in Eq. (17) is the possibility of one of the main diagonal terms of matrix of mass to become zero when angle φ is zero. This singularity occurs when the rod of the pendulum is at the vertical direction. This problem is circumvented by including an incremental value (ε) to avoid the denominator of Eq. (18) become zero.

$$\ddot{\theta}(t) = \frac{asin\theta(t)\ddot{x}(t) - m_p acos\theta(t)\ddot{y}(t) - 2al\dot{\varphi}(t)\dot{\theta}(t)cos\varphi(t)}{m_p^2 l^2 [sin\varphi(t)]^2 + \varepsilon} \tag{18}$$

As reported by Pinheiro and Battista (2012), the incremental value can be neglected if the external force is harmonic and out of phase; because the motion of the pendulum mass at the tip of the inclined rod follows an elliptical trajectory. In this case, just an initial condition should be provided to the angle φ.

Nevertheless, in a generic situation where a random external force is acting on the structure it is possible that the rod passes by the vertical position, and then the incremental value (ε) is required. In this work, it is assumed as $\varepsilon = 1.10^{-9}$.

7. Performance evaluation of the nonlinear pendulum device

The performance evaluation of the mathematical models of the NLPD was made by means of a parametric study to find out the optimum parameters of the pendulum controller such as its mass, damping and length of the rod.

The coupled system of differential equations was solved numerically with the Runge-Kutta method and the influence of the controller's parameters were assessed in terms of the reduction factor defined herein as the ratio between the controlled and uncontrolled response of the structure in terms of maximum amplitudes of displacements.

The modal properties of the structure associated with the 1st vibration mode were determined from the 3D finite element model (FEM) and are presented in Table 4. The corresponding modal components of the exciting forces generated, mainly, by the piston effect caused by the turbulent flow of the fluid and solid particles colliding with the pipes of the FCC unit are given in Table 5.

Experimental measured displacements of the bottle-like tower (see Fig. 4(a)) suggest the modeling of the components of the external forces as harmonic loads, as written in Eq. (19), with dominant excitation frequency $f_e \approx$ 1.01 Hz.

$$F(t) = F_0 sin(2\pi f_e t + \alpha) \tag{19}$$

where, F_0 is the amplitude of the excitation force, f_e is the excitation frequency and α is the phase angle (Table 5).

The performance of the 2D and 3D mathematical models are compared in terms of the reduction factor. For that the maximum planar displacements at the top of the bottle like tower, obtained for each model and for a given set of NLP parameters, are decoupled in the directions X and Y and analysed separately.

7.1 Pendulum performance as function of mass ratio

To evaluate the performance of the nonlinear pendulum (NLP) as a function of the mass ratio, the length of the rod

Table 4 Modal properties of the structure

Modal properties	X-direction	Y-direction
m_s (ton)	2327.00	696.00
k_s (kN/m)	93712.79	24278.66
c_s (kNs/m)	1476.72	411.07
f_s (Hz)	1.01	0.94

Table 5 Exciting force data

	X-direction	Y-direction
F_0 (ton)	50.0	25.0
f_e (Hz)	1.01	1.01
α (rad)	0.0	0.5
	X-direction	Y-direction

$(l = 0.24\,m)$ and the damping ratio $(\xi_p = 0.01)$ of the pendulum were both kept constant.

The achieved results in terms of horizontal displacements in directions X and Y show a great reduction in the structure's vibrations amplitudes in X-direction for increasing values of the mass ratio (m_p/m_{sx}) in the range 0.5%-1.0%, as shown in Fig. 11. Similar results were also reported by Pinheiro and Battista (2012) for the same range of values of the ratio between the pendulum mass and the modal mass of the structure.

Comparing the results obtained from the two different mathematical models proposed herein, it can be noted the better correlation in X-direction in relation to the Y-direction. This probably occurs as consequence of the lower modal mass in Y direction that is strongly influenced by the motion in X-direction. The 2D mathematical model does not show this because the motion in the X and Y directions are uncoupled.

7.2 Pendulum performance as function of rod length

Fig. 12 shows the reduction factor related to the vibration amplitudes at the top of the FCC unit as a function of the length of the pendulum's rod while the mass ratiom_p/m_{sx} and the damping ratio are kept constant with values 0.005 and 1.0%, respectively.

As could be expected, the greatest effectiveness of the pendulum device is reached when it is tuned both to the excitation force frequency and to the natural frequency of the structure. It can be noted in Fig. 12 that for some lengths of the pendulum's rod it may occur an increase in the vibration amplitudes of the structure in Y-direction caused by the detuning between pendulum, structure and excitation force frequencies. Moreover, as indicated by dashed lines in this figure, the natural frequency of the simple pendulum $(\omega = \sqrt{l/g})$ provides a good estimation of the natural frequency for both 2D and 3D NLP mathematical models.

7.3 Pendulum performance as function of damping

To evaluate the performance of the nonlinear pendulum (NLP) as a function of its damping ratio, the mass of the pendulum $(m_p/m_{sx} = 0.005)$ and length of the rod $(l = 0.24\,m)$ were fixed while varying damping ratio. For the motion of the structure in X direction, which is the direction with greater amplitudes of displacements, the optimum damping ratio values were found in between 0.5% and 1.0%, as shown in Fig. 13.

In Y-direction, there is a large difference between the reduction factor obtained with the 2D and 3D mathematical models for different pendulum's damping ratios. It occurs

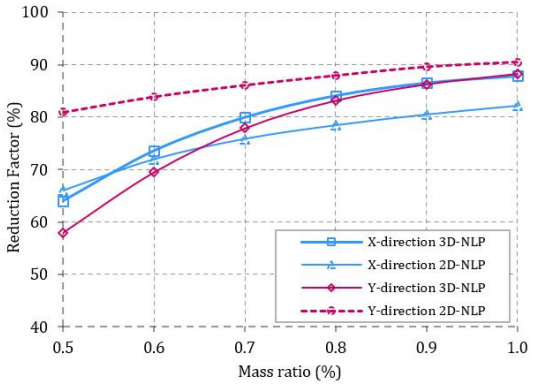

Fig. 11 Pendulum performance as a function of mass ratio

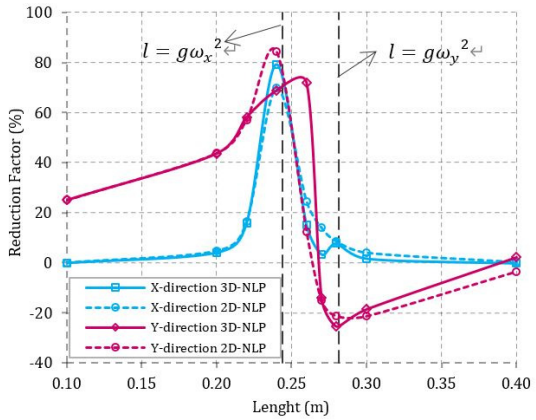

Fig. 12 Pendulum performance as a function of rod length

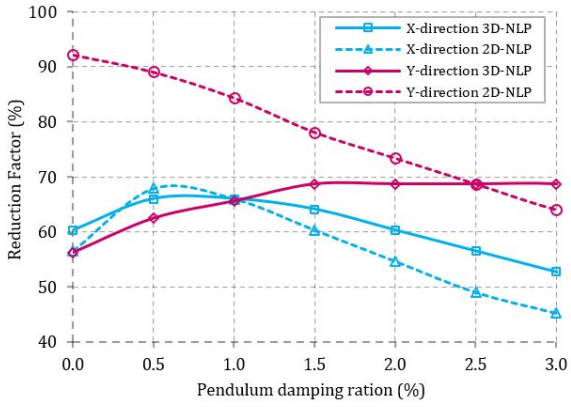

Fig. 13 Pendulum performance as a function of damping ratio

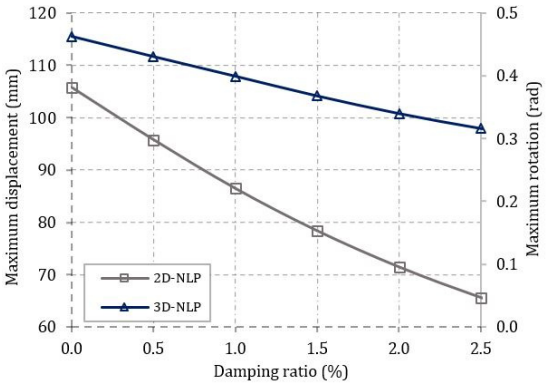

Fig. 14 Variation maximum pendulum mass displacement and rod rotation with increasing damping

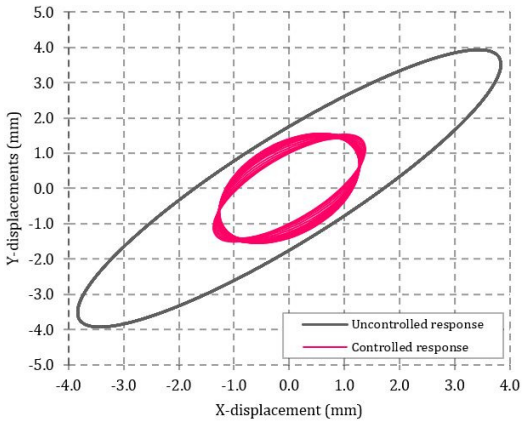

Fig. 15 Trajectories of the controlled and uncontrolled displacement at the top of bottle-like tower

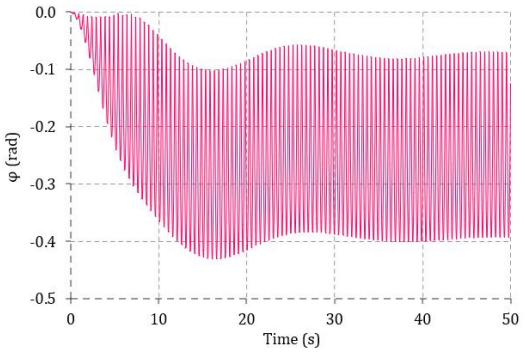

Fig. 16 Rotation of the pendulum rod in relation to Z-axis

specially because in 3D mathematical model the motion of the structure in Y-direction is influenced by the motion of the structure in X-direction for which the maximum reduction factor is reached for low values of the damping ratio (0.5%-1.0%), consequently a more significative reduction of the displacements in Y-direction is observed for this range of values.

To simulate the amplitudes of vibrations reached by the pendulum mass and its installation feasibility, Fig. 14 shows the maximum displacement and rotation of the NLP controller to different damping ratios. As expected, the maximum displacement of the pendulum mass occurs to low values of damping ratio. For high damping ratios the motion of the NLP controller tends to be locked in phase with the motion of the structure, becoming ineffective. On the other hand, for low values of damping ratio the lateral displacement of the pendulum mass may reach large amplitudes jeopardizing the installation of the control device.

The nonlinear mathematical model equations may be linearized for some conditions. According to Fallahpasand *et al*. (2015), for rotation amplitudes of the NLP larger than 0.2 rad, as it is shown in Fig. 14 for the case in focus, the linearization might contain enormous errors.

7.4 Designed controller parameters

Table 6 presents the NLP's optimum parameters determined by means of a parametric study and guided by practical aspects regarding the installation of the control device in the FCC unit.

The dynamic response of the FCC unit was evaluated in terms of the motion amplitudes at the level 39 m of the bottle-like tower. Fig. 15 shows the motion trajectories of the uncontrolled and controlled structure obtained with the 3D mathematical model and considering the design parameters of the pendulum device given in Table 6.

Table 6 Modal properties of the pendulum device

Modal properties	Value
m_p (ton)	11.635
l (m)	0.244
ξ_p (%)	1.00

Fig. 16 shows the motion of the pendulum mass in terms of rotation of the rod in relation to the vertical axis, reaching a maximum angle of approximately -0.43 rad. This rotation angle corresponds to maximum lateral displacements of NLP mass of approximately 107 mm.

8. Assessment of the proposed solutions

The assessment of the two proposed solutions to improve the dynamic behavior and to attenuate the vibrations of the FCC unit are evaluated in terms of lifetime of a critical welded joint in the "neck" of the reactor-regenerator tower, as indicated in Fig. 17.

Three simulations were performed to determine the stress variation in the components of the FCC unit: (i) uncontrolled structure, (ii) structure strengthened (Fig. 7) with four curved steel tubular struts; (iii) controlled structure with a nonlinear pendulum (Fig. 8). The first simulation consisted of applying equivalent forces to the numerical model of the uncontrolled structure to obtain the same displacement values of those measured in experimental tests and consequent stress at the critical welded joint. The same equivalent forces were applied to the two models of the controlled structure. The results in terms of displacements of the controlled structure were

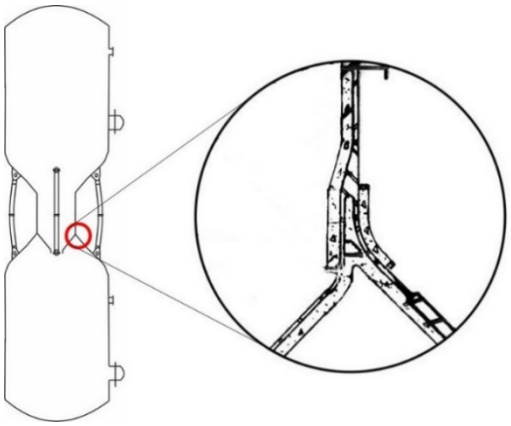

Fig. 17 Critical welded joint at the "neck" of the reactor-regenerator tower

compared to those of uncontrolled one, and the percentual ratio between them was applied to the stress values obtained from the uncontrolled structure.

The strengthening of the "neck" by means of the installation of four struts results in a reduction of 18% in stress values at the critical welded joint while the installation of the non-linear pendulum results in a reduction of 50%.

The fatigue analysis was performed with the application of the Palgrem-Miner rule combined with the classical SN curves (Gurney 1976) used in bridges design codes (BS 5400 1980) and offshore structures guidelines (Mansour *et al*. 1996).

The welded joints were considered well executed and flawless at the beginning of the lifetime of the structure. The rainflow method (Matsuishi and Endo 1968) was employed as the cycle counting algorithm applied to the stress time history.

According to the refinery's engineers own records the structure had been in full service for 27 years at the date of the work reported herein and in the last five years vibration problem became increasingly evident. Dynamic response amplitudes caused by the hydrodynamic piston effect were strongly increased in periodical operational procedures totalizing around 10 days each year.

Based on these records it was considered in the fatigue analyses maximum amplitudes equal to ±0.5 mm for the first 22 years. However, in the last 5 years, the amplitude was considered equal to ±0.5 mm along 355 days of the year and along the remaining 10 days an amplitude equal to ±3.25 mm. For the uncontrolled structure, these amplitudes are repeated for the next years until the cumulative damage reaches one and the first crack that is expected to happen. For the controlled structure, the stress amplitudes during the next years reduced 18% for the strengthened structure and 50% for the structure with the attached pendulum.

Considering in a conservative manner that the focused welded joint is class E and the stress concentration factor is 2.5, the fatigue analysis yields the following results for the structure's lifetime extension: 7.2 years for the uncontrolled structure, 13 years for the strengthened structure and 57.5 years for the controlled structure with the conceived nonlinear pendulum controller.

9. Final remarks

A nonlinear spatial pendulum (NLP) controller was designed to attenuate the vibration amplitudes of the FCC unit caused by intermittent fluid dynamic forces due to turbulent flow in the pipe system.

Dynamic responses were carried out for the uncontrolled and controlled structural system and the obtained results were discussed in terms of the reduction factor of planar displacement amplitudes at the top of the controlled reactor-regenerator tower in relation to the uncontrolled counterpart.

It is shown that the simplified 2D mathematical model of the NLP controller can be very useful to one have some insight in relation to the controlled system dynamic response. However, it is neither adequate nor sufficient as it is the 3D mathematical model to simulate the spatial coupled motion of the structure and the NLP and to demonstrate the effectiveness of NLP controller in reducing substantially the dynamic response amplitudes.

Reduction factors of more than 60% of the oscillation amplitudes of the bottle-like tower were obtained by considering the optimum parameters of the proposed NLP controller.

A fatigue analysis of the critical welded joint located at the "neck" of the bottle-like tower was performed for the uncontrolled and the controlled structure considering, respectively: (i) the strengthening of the "neck" and (ii) installation of the nonlinear pendulum at the top of the reactor-regenerator tower.

Reductions of 18% and 50% in the stress values at the critical welded joint in the "neck" were obtained, respectively, for the strengthened structure and for the structure provided with the nonlinear pendulum device. The lifetime extension of the welded joint jumped from 7.2 years for the uncontrolled structure to 13 years for the strengthened one and 57.5 years for the controlled structure with the pendulum device.

Acknowledgments

The authors acknowledge Brazilian National research Council - CNPQ and Petrobras BR for the financial support.

References

Ali, M.F., El Ali, B.M. and Speight, J.G. (2005), *Handbook of Industrial Chemistry*, McGraw-Hill Companies, New York, NY, USA.

Alih, S.C., Vafaei, M., Ismail, N. and Pabarja, A. (2018), "Experimental study on a new damping device for mitigation of structural vibrations under harmonic excitation", *Earthq. Struct*., *Int. J*., **14**(6), 567-576. https://doi.org/10.12989/eas.2018.14.6.567

An, Q., Chen, Z., Ren, Q., Liu, H. and Yan, X. (2015), "Control of human-induced vibration of an innovative CSBS-CSCFS", *J. Constr. Steel Res*., **115**, 359-371. https://doi.org/10.1016/j.jcsr.2015.08.030

Battista, R.C., Pfeil, M.S., Carvalho, E.M.L. and Varela, W.D. (2018), "Double controller of wind induced bending oscillations in telecom towers", *Smart Struct. Syst*., *Int. J*., **21**(1), 99-111.

https://doi.org/10.12989/sss.2018.21.1.099
BS 5400: Part 10 (1980), Steel, concrete and composite bridges, Code of practice for fatigue, London: BSI.
Cao, L., Li, C. and Chen, X. (2021), "Performance of multiple tuned mass dampers-inerters for structures under harmonic ground acceleration", *Smart Struct. Syst.*, *Int. J.*, **26**(1), 49-61. https://doi.org/10.12989/sss.2020.26.1.049
Duran, B., Tunaboyu, O., Kaplan, O. and Avsar, O. (2018), "Effectiveness of seismic repairing stages with CFRPs on the seismic performance of damage RC frames", *Struct. Eng. Mech.*, *Int. J.*, **67**(3), 233-244. https://doi.org/10.12989/sem.2018.67.3.233
Fallahpasand, S., Dardel, M., Pashaei, M.H. and Daniali, H.R.M. (2015), "Investigation and optimization of nonlinear pendulum vibration absorber for horizontal vibration suppression of damped system", *Struct. Des. Tall Special Build.*, **24**, 873-893. https://doi.org/10.1002/tal.1216
Gerges, R.R. and Vickery, B.J. (2005), "Optimum design of pendulum-type tuned mass dampers", *Struct. Des. Tall Special Build.*, **14**, 353-368. https://doi.org/10.1002/tal.273
Gurney, T.R, (1976), "Fatigue design rules for welded steel joints", *Weld. Inst. Res. Bull.*, May, pp. 115-124.
Ikeda, T., Harata, Y. and Takeeda, A. (2017), "Nonlinear responses of spherical pendulum vibration absorbers in tower like 2DOF structures", *Nonlinear Dyn.*, **88**, 2915-2932. https://doi.org/10.1007/s11071-017-3421-5
Letzsch, W. (2015), "Fluid Catalytic Cracking (FCC) in Petroleum Refining", In: *Handbook of Petroleum Processing*, (Treese S., Pujadó P., Jones D. Eds.), Springer, Cham.
Lin, C.-S., Zhang, J., Wang, J.-F. and Li, C.-C. (2019), "Vibration control for serviceability enhancement of offshore platforms against environmental loadings", *Smart Struct. Syst.*, *Int. J.*, **24**(3), 402-414. https://doi.org/10.12989/sss.2019.24.3.403
Mansour, A.E., Wirsching, P.H., White, G.J. and Ayyub, B.M. (1996), "Probability-Based Ship Design: Implementation of Design Guidelines", SSC 392, NTIS, Washington, D.C., 200 pages.
Matsuishi, M. and Endo, T. (1968), "Fatigue of metals subjected to varying stress-fatigue lives under random loading", *Proc. Kyushu District Meeting*, JSEM, Fukuoka, Japan, pp. 37-40.
Medeiros, J., Battista R.C. and Carvalho, E.M.L. (2010), "Fluid Catalytic Cracking (FCC) Riser Submitted to Flow Induced Vibration Fatigue Life Estimation", *XXIX Computational Methods for the Analysis and Design of Offshore*, Buenos Aires, Argentina, November.
Nguyen, T., Gad, E. and Wilson, J. (2014), "Mitigation footfall-induced vibration in long-span floors", *Austral. J. Struct. Eng.*, **15**(1), 97-109.
Pinheiro, M.A.S. and Battista, R.C. (2012), "Efficiency of a spatial pendulum in vibration control", *XXXV Jornadas Sulamericanas de Engenharia Estrutural*, Rio de Janeiro, Brazil, September. [In Portuguese]
Pinheiro, C.I.C., Fernandes, J.L., Domingues, L., Chambel, A.J.S., Graça, I., Oliveira, N.M.C., Cerqueira, H.S. and Ribeiro, F.R. (2011), "Fluid Catalytic Cracking (FCC) Process Modeling, Simulation, and Control", *Ind. Eng. Chem. Res.*, **51**, 1-29. https://doi.org/10.1021/ie200743c
Roffel, A.J., Narasimhan, S. and Haskett, T. (2013), "Performance of pendulum tuned mass dampers in reducing the responses of flexible structures", *J. Struct. Eng.*, **139**, 04013019. https://doi.org/10.1061/(ASCE)ST.1943-541X.0000797
Sado, D., Freunlich, J. and Dudanowicz, A. (2016), "The dynamics of a coupled mechanical system with spherical pendulum", *Vib. Phys. Syst.*, **27**, 309-316.
Shahabi, A.B., Ahari, Z. and Barghian, M. (2020), "Suspended columns for seismic isolation in structures (SCSI): experimental and numerical studies", *Earthq. Struct.*, *Int. J.*, **19**(1), 17-28. https://doi.org/10.12989/eas.2020.19.1.17
Sharma, R.K., Domala, V. and Sharma, R. (2019), "Dynamic analysis of an offshore jacket platform with a tuned mass damper under the seismic and ice loads", *Ocean Syst. Eng.*, *Int. J.*, **9**(4), 369-390. https://doi.org/10.12989/ose.2019.9.4.369
Speight, J.G. (2006), *The Chemistry and Technology of Petroleum*, Taylor & Francis Group (LCC), Laramie, WY, USA.
Sun, C., Jahangiri, V. and Sun, H. (2019), "Performance of a 3D pendulum tuned mass damper in offshore wind turbines under multiple hazards and system variations", *Smart Struct. Syst.*, *Int. J.*, **24**(1), 53-65. https://doi.org/10.12989/sss.2019.24.1.053
Viet, L.D. and Park, Y. (2011), "Vibration control of the axisymmetric spherical pendulum by dynamic vibration absorver moving in radial direction", *J. Mech. Sci. Tech.*, **25**(7), 1703-1709. https://doi.org/10.1007/s12206-011-0418-8
Vogt, T.T.C. and Weckhuysen, B.M. (2015), "Fluid catalytic cracking: recent developments on the grand old lady zeolite catalysis", *Chem. Soc. Rev.*, **44**, 7342-7370. https://doi.org/10.1039/C5CS00376H
Wang, L., Shi, W., Zhou, Y. and Zhang, Q. (2020), "Semi-active eddy current pendulum tuned mass damper with variable frequency and damping", *Smart Struct. Syst.*, *Int. J.*, **25**(1), 65-80. https://doi.org/10.12989/sss.2020.25.1.065
Zahrai, S.M. and Froozanfar, M. (2019), "Performance of passive and active MTMDs in seismic response of Ahvaz calbe-stayed bridge", *Smart Struct. Syst.*, *Int. J.*, **23**(5), 449-466. https://doi.org/10.12989/sss.2019.23.5.449
Zhang, R., Cao, Y. and Dai, K. (2021), "Response control of wind turbines with undergrounded tuned mass inerter system (TMIS) under wind loads", *Wind Struct.*, *Int. J.*, **32**(6), 573-586. https://doi.org/10.12989/was.2021.32.6.573
Zhu, L-H., Li, G. and Dong, Z-Q. (2021), "Dynamic test and numerical simulation on avoiding the weak-story failure mechanism in structures using LSFDs", *Steel Compos. Struct.*, *Int. J.*, **40**(2), 175-191. https://doi.org/10.12989/scs.2021.40.2.175

CC